JACS
JOURNAL OF THE AMERICAN CHEMICAL SOCIETY
Article
pubs.acs.org/JACS

# Self-Assembling Nano-Architectures Created from a Protein Nano-Building Block Using an Intermolecularly Folded Dimeric *de Novo* Protein

Naoya Kobayashi,[†,⊥,‡] Keiichi Yanase,[¶,§] Takaaki Sato,[¶,§] Satoru Unzai,[∥] Michael H. Hecht,[#] and Ryoichi Arai*[,†,⊥,▽]

[†]Department of Bioscience and Textile Technology and [¶]Department of Materials Science and Engineering, Interdisciplinary Graduate School of Science and Technology and [⊥]Division of Applied Biology and [§]Division of Chemistry and Materials, Faculty of Textile Science and Technology, Shinshu University, Ueda, Nagano 386-8567, Japan

[‡]Japan Society for the Promotion of Science, Chiyoda, Tokyo 102-8471, Japan

[∥]Graduate School of Medical Life Science, Yokohama City University, Tsurumi, Yokohama, Kanagawa 230-0045, Japan

[#]Department of Chemistry, Princeton University, Princeton, New Jersey 08544, United States

[▽]Institute for Biomedical Sciences, Interdisciplinary Cluster for Cutting Edge Research, Shinshu University, Matsumoto, Nagano 390-8621, Japan

Supporting Information

**ABSTRACT:** The design of novel proteins that self-assemble into supramolecular complexes is an important step in the development of synthetic biology and nanotechnology. Recently, we described the three-dimensional structure of WA20, a *de novo* protein that forms an intermolecularly folded dimeric 4-helix bundle (PDB code 3VJF). To harness the unusual intertwined structure of WA20 for the self-assembly of supramolecular nanostructures, we created a protein nanobuilding block (PN-Block), called WA20-foldon, by fusing the dimeric structure of WA20 to the trimeric foldon domain of fibritin from bacteriophage T4. The WA20-foldon fusion protein was expressed in the soluble fraction in *Escherichia coli*, purified, and shown to form several homooligomeric forms. The stable oligomeric forms were further purified and characterized by a range of biophysical techniques. Size exclusion chromatography, multiangle light scattering, analytical ultracentrifugation, and small-angle X-ray scattering (SAXS) analyses indicate that the small (S form), middle (M form), and large (L form) forms of the WA20-foldon oligomers exist as hexamer (6-mer), dodecamer (12-mer), and octadecamer (18-mer), respectively. These findings suggest that the oligomers in multiples of 6-mer are stably formed by fusing the interdigitated dimer of WA20 with the trimer of foldon domain. Pair-distance distribution functions obtained from the Fourier inversion of the SAXS data suggest that the S and M forms have barrel- and tetrahedron-like shapes, respectively. These results demonstrate that the *de novo* WA20-foldon is an effective building block for the creation of self-assembling artificial nanoarchitectures.

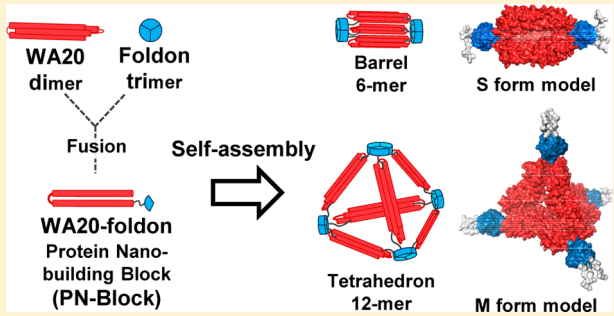


## INTRODUCTION

Living organisms are maintained by various self-assembling biomolecules including proteins, nucleic acids, sugars, and lipids. The chemical reconstitution of living matter is one of the ultimate goals of chemistry and synthetic biology, and rational design of artificial biomacromolecules that self-assemble into supramolecular complexes is an important step toward achieving this goal.

In recent years, DNA origami has been developed to design and create various nanostructures.[1−3] The base complementarity of DNA can be used to design rationally artificial nanostructures with versatile two-dimensional (2D) and three-dimensional (3D) shapes, such as polyhedra.[4] However, nucleic acids generally consist of only four types of bases, A, T, G, and C, and the limited number of combinations and chemical features might restrict the potential to produce advanced functions.

Proteins consist of 20 types of amino acids, allowing a greater number of chemical properties. Moreover, the enormous varieties of possible sequence combinations expand the probabilities to create diverse and advanced functions. In nature, proteins perform the complex and functional tasks in living organisms because proteins can form intricate and refined tertiary and quaternary structures with versatile chemical properties and functionalities.

**Received:** April 9, 2015
**Published:** June 29, 2015





DOI: 10.1021/jacs.5b03593
J. Am. Chem. Soc. 2015, 137, 11285−11293

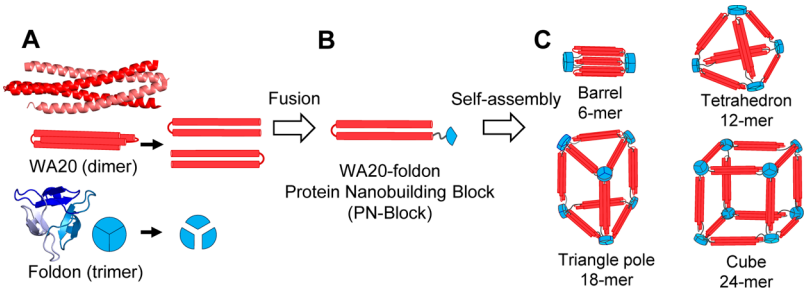


**Figure 1.** Schematics of construction and assemblies of the WA20-foldon fusion protein as a PN-Block. (A) Ribbon representation (see also Figure S1, Supporting Information) and schematics of the intermolecularly folded dimeric WA20 (PDB code 3VJF),[5] shown in red, and trimeric foldon domain of T4 phage fibritin (PDB code 1RFO),[6] shown in blue. (B) Construction of the WA20-foldon fusion protein as a PN-Block. (C) Schematics of a nanoarchitecture design by expected self-assemblies of the WA20-foldon. In stable self-assembling complexes, the WA20-foldon is expected to form highly symmetric oligomers in multiples of 6-mer because of the combination of the WA20 dimer and foldon trimer.

The design of *de novo* proteins is substantially complicated because of the contribution of many cooperative and long-range interactions. *De novo* protein design and engineering have been performed with mainly two motivations: (1) recapitulation of natural systems to ultimately test our understanding of the principles of protein structure and function and (2) construction of tailor-made proteins as an essential step toward applied biotechnology. Research on *de novo* protein design has progressed toward the construction of novel proteins emanated mainly from three approaches: (1) rational and computational design,[7−9] (2) combinatorial methods,[10] and (3) semirational approaches, including elements of both rational design and combinatorial methods.[11,12]

As a semirational approach, the binary code strategy has been developed to produce focused libraries of *de novo* proteins designed by the binary patterning of polar and nonpolar residues, and $\alpha$-helix or $\beta$-sheet *de novo* proteins have been created.[11−14] From a third-generation library of *de novo* 4-helix bundle proteins designed by binary patterning, a stable and functional *de novo* protein called WA20 was obtained.[15,16] Recently, we solved the crystal structure of the *de novo* protein WA20, revealing an unusual 3D-domain-swapped dimeric structure with a intermolecularly folded 4-helix bundle.[5] (3D domain swapping is a mechanism of exchanging one structural domain of a protein monomer with that of the identical domain from a second monomer, resulting in an intertwined oligomer.[17,18]) Each WA20 monomer ("nunchaku"-like structure), which comprises two long $\alpha$-helices, intertwines with the helices of another monomer (Figure 1A and Figure S1, Supporting Information). This unusual intertwined topology was first found in the topology-changed structure of the Rop A31P mutant,[19] which was thermodynamically destabilized.[20] The structure of WA20 is stable (melting temperature, $T_m$ = ~70 °C) and forms a simple rod-like shape with ~8 nm length and ~3 nm diameter.[5] The stable, simple, and unusual intermolecularly folded structure of the *de novo* protein WA20 raises the possibility of application to basic framework tools in nanotechnology and synthetic biology.

In recent years, several approaches to design artificial self-assembled protein complexes have been developed:

- 3D domain-swapped dimers and fibrous oligomers[21]
- Nanostructures including cages,[22−24] filaments,[22] and lattices,[25] constructed from fusion proteins designed by symmetric self-assembly
- Self-assembling fibers,[26−28] nanostructures,[29] and cages[30] constructed from designed coiled-coil peptide modules
- Metal-directed self-assembling protein complexes[31,32]
- A single-chain polypeptide tetrahedron assembled from coiled-coil segments[33]
- Computationally designed self-assembling protein nanomaterials with atomic level accuracy[34,35]
- Other approaches (see refs 36−42)

In this study, to apply the simple, stable, and characteristic intermolecularly folded dimeric structure of WA20 to construct supramolecular nanostructures, we designed and constructed a WA20-foldon—a fusion protein of the dimeric *de novo* protein WA20[5] and a trimeric foldon domain[6,43] of fibritin from bacteriophage T4—as a simple and versatile nanobuilding block (Figure 1). In the nanoarchitectures, the parts of the WA20 and foldon domains resemble a rectilinear framework/edge and corner vertex/node, respectively (Figure 1C). Here, we report the design and construction of the WA20-foldon fusion protein as a novel protein nanobuilding block (PN-Block) and demonstrate its characteristic self-assembling nanoarchitectures.

## MATERIAL AND METHODS

**Construction of Expression Plasmid of WA20-Foldon.** The DNA fragment encoding the *de novo* protein WA20 was prepared from plasmid pET3a-WA20[5,16] by polymerase chain reaction (PCR) using KOD-Plus-Neo DNA polymerase (Toyobo, Osaka, Japan) and primers, T7 promoter primer and WA20RV_*Hin*dIII (Table S1, Supporting Information). The amplified fragment was digested by *Nde*I and *Hin*dIII and cloned into pET32b(+) (Merck Millipore, Darmstadt, Germany) between the *Nde*I and *Hin*dIII sites to construct the plasmid pET-WA20, i.e., the Trx tag was removed and replaced with WA20. The DNA fragment encoding the foldon domain (residues 458−483 in T4 phage fibritin) was prepared by annealing and extension reactions with the two synthesized oligonucleotides (Foldon_*Hin*dIII-*Not*I_FW and Foldon_*Xho*I_RV) (Table S1, Supporting Information). The DNA fragment encoding the foldon domain digested *Hin*dIII and *Xho*I and cloned into pET-WA20 between the *Hin*dIII and *Xho*I sites to give the expression plasimid pET-WA20-foldon. The amino acid sequence of the WA20-foldon fusion protein with a $His_6$ tag at the C terminal is shown in Figure S2 (Supporting Information).

**Protein Expression and Purification of WA20-Foldon.** The WA20-foldon protein with a $His_6$ tag was expressed in *Escherichia coli* BL21 Star(DE3) (Invitrogen, Carlsbad, CA) harboring pET-WA20-foldon using LB broth, Lennox (Nacalai Tesque, Kyoto, Japan) with 50 $\mu$g/mL ampicillin sodium salt at 37 °C. The expression was induced with 0.2 mM isopropyl $\beta$-D-1-thiogalactopyranoside at $OD_{600}$ (optical density at 600 nm) = ~0.8, and cells were further cultured for 3−4 h at 37 °C. The protein was extracted from the harvested cells by sonication in a lysis buffer (50 mM sodium phosphate buffer (pH 7.0)


DOI: 10.1021/jacs.5b03593
J. Am. Chem. Soc. 2015, 137, 11285−11293

containing 300 mM NaCl, 10% glycerol). The protein was purified by immobilized metal ion affinity chromatography (IMAC) with a HisTrap HP column (GE healthcare, Little Chalfont, UK) and eluted using a linear gradient of imidazole (equilibration buffer: 20 mM sodium phosphate buffer (pH 7.4) containing 500 mM NaCl, 200 mM L-ArgHCl, 10% glycerol, and 20 mM imidazole; elution buffer: 20 mM sodium phosphate buffer (pH 7.4) containing 500 mM NaCl, 200 mM L-ArgHCl, 10% glycerol, and 500 mM imidazole). The protein samples were concentrated with Amicon ultra centrifugal filters (Merck Millipore). Each form of the WA20-foldon protein was further purified repeatedly by size exclusion chromatography (SEC) (20 mM HEPES buffer (pH 7.5) containing 100 mM NaCl, 200 mM L-ArgHCl, and 10% glycerol) with HiLoad 16/600 Superdex 200 pg and Superdex 200 Increase 10/300 GL columns (GE healthcare).

**SEC Multi-Angle Light Scattering (SEC-MALS).** SEC-MALS experiments were performed using a 1260 Infinity HPLC system (Agilent Technologies, Santa Clara, CA) equipped with a Superdex 200 Increase 10/300 GL column, which was connected in line with a miniDAWN TREOS multiangle static light-scattering detector (Wyatt Technology, Santa Barbara, CA). The data were collected in phosphate buffered saline (PBS, pH 7.4:1 mM $KH_2PO_4$, 3 mM $Na_2HPO_4$, and 155 mM NaCl) at 20 °C and analyzed using ASTRA 6 software (Wyatt Technology). The $dn/dc$ value (0.185 mL/g) was generally used for proteins, and the extinction coefficient (0.913 mL $mg^{-1}$ $cm^{-1}$) for the WA20-foldon was calculated from the amino acid sequence.[44]

**Analytical Ultracentrifugation (AUC).** AUC experiments were performed at 20 °C using an analytical ultracentrifuge, Optima XL-I (Beckman Coulter, Brea, CA) with a An-50 Ti rotor. For sedimentation velocity experiments, cells with a standard Epon two-channel centerpiece and sapphire windows were used. The sample (400 μL) and reference buffer (420 μL; 20 mM HEPES buffer (pH 7.5) containing 100 mM NaCl, 200 mM L-ArgHCl, and 10% glycerol) were loaded into the cells. Absorbance scans at 280 nm were collected at 10 min intervals during sedimentation at 50 × $10^3$ rpm. The sedimentation velocity experiments were performed at protein concentrations of 1.2, 0.6, and 0.3 mg/mL. Partial specific volume of the protein was calculated from standard tables using the SEDNTERP program.[45] The solvent density (1.0472 g/$cm^3$) and solvent viscosity (1.5639 cP) were determined using DMA 4500 M and AMVn (Anton Paar, Graz, Austria), respectively. The resulting scans were analyzed using the continuous distribution ($c(s)$) analysis module in the SEDFIT program (version 14.7g).[46] Sedimentation coefficient increments of 200 were used in the appropriate range for each sample. The frictional coefficient was allowed to float during fitting. The weight-average sedimentation coefficient was obtained by integrating the range of sedimentation coefficients in which peaks were present. The values of sedimentation coefficient were corrected to 20 °C in pure water ($s_{20,w}$).

Sedimentation equilibrium experiments were carried out in cells with a six-channel centerpiece and quartz windows at 20 °C. The sample concentrations were 0.6, 0.3, and 0.15 mg/mL. Data were obtained at 4, 9, and 20 × $10^3$ rpm. A total equilibration time of 48 h was used for each speed, with absorbance scans at 280 nm taken every 4 h to ensure that equilibrium had been reached. Data analysis was performed by global analysis of data sets obtained at different loading concentrations and rotor speeds using SEDPHAT program (version 10.58d).[47]

**Small-Angle X-ray Scattering (SAXS).** SAXS measurements were performed on the WA20-foldon oligomers, chicken egg white lysozyme (Wako Pure Chemical Industries, Osaka, Japan), and WA20[5] in 20 mM HEPES buffer (pH 7.5) containing 100 mM NaCl, 200 mM L-ArgHCl, 10% glycerol, and 1 mM dithiothreitol at 4 °C (Table S2, Supporting Information). The SAXS measurements were performed by SAXSess $mc^2$ (Anton Paar) with a SAXSess camera (Anton Paar) attached to a sealed-tube anode X-ray generator (GE Inspection Technologies, Huerth, Germany). The line-shaped and monochromatic X-ray beams of CuK$\alpha$ radiation ($\lambda$ = 0.1542 nm) were provided by a Göbel mirror and a block collimator. Liquid samples were filled into a temperature-controlled vacuum-tight quartz capillary cell. An imaging plate detector that recorded the primary beams attenuated by a semitransparent beam stop and the scattered X-rays was read out by a Cyclone Phosphor System (PerkinElmer, Waltham, MA). The 2D scattering patterns were integrated into one-dimensional scattering intensities, $I(q)$, as a function of the magnitude of the scattering vector, $q = (4\pi/\lambda)\sin(\theta/2)$, using the SAXSQuant program (Anton Paar), where $\theta$ is the total scattering angle. All $I(q)$ data were normalized to have a uniform primary intensity at $q = 0$ for transmission calibration. The background scattering contributions from the capillary and solvent were corrected. The absolute intensity calibration was performed by referring to water as a secondary standard.[48]

Generally, the scattering intensity for a colloidal dispersion is given by the product of the form factor, $P(q)$, and the structure factor, $S(q)$:

$$I(q) = nP(q)S(q)$$

where $n$ is the number density of the particle. If interparticle interactions including the excluded volume effect and electrostatic interaction can be neglected (i.e., $S(q) = 1$), the scattering intensity is proportional to the form factor. Our experimental condition can be regarded as a situation in which the structure factor is almost unity, i.e., $I(q) \approx n\,P(q)$, because of a low protein concentration and a high salt concentration of the solvent. The form factor is given by the Fourier transformation of the pair-distance distribution function, $p(r)$, which describes the size and shape of the particle:

$$P(q) = 4\pi \int_0^{D_{max}} p(r)\frac{\sin qr}{qr}\mathrm{d}r$$

where $D_{max}$ is the maximum intraparticle distance. To obtain $p(r)$ of the proteins and their self-assemblies using a virtually model-free routine, we used the indirect Fourier transformation (IFT) technique.[49−51] The forward absolute scattering intensity, $I(q \to 0)$, was extrapolated from the data. The radius of gyration, $R_g$, was estimated by the Guinier approximation.[50]

**Rigid-Body Modeling of Oligomeric Structures of WA20-Foldon.** The rigid-body models of WA20-foldon oligomeric structures were constructed using the program COOT[52] based on the crystal structure of WA20 [protein data bank (PDB) code, 3VJF][5] and the solution structure of the foldon domain (PDB code, 1RFO)[6] with a consideration of their N- and C-terminal directions and two- and three-fold symmetries. The rigid-body models were manually and iteratively refined to minimize differences in the $p(r)$ and $I(q)$ calculated from the models and those obtained from SAXS experiments (Figures S3−S5, Supporting Information).

**Calculation of *ab Initio* Low-Resolution Shapes of WA20-Foldon.** Low-resolution supramolecular shapes were reconstructed from the SAXS intensity profiles using an *ab initio* procedure of the program DAMMIN[53] in the ATSAS program package.[54] Using dummy atom minimization (DAMMIN), a protein molecule is approximated by densely packed small spheres (dummy atoms). Because the low-resolution *ab initio* modeling procedure does not consider the internal structure, relatively low-angle data ($qR_g < 7$) were used. Simulated annealing calculations were performed several times to determine a configuration that fits the SAXS data, starting from the dummy atoms placed at random coordinates within the search space, a sphere of diameter $D_{max}$, with/without a consideration of two- and/or three-fold symmetry constraints.

## RESULTS AND DISCUSSION

**Design of WA20-Foldon as a PN-Block to Construct Self-Assembling Nanostructures.** As shown in Figure 1, to construct self-assembling nanostructures, the first PN-Block, the WA20-foldon, which utilized the unusual intermolecularly folded dimeric *de novo* protein WA20 as a framework, was designed by reference to the "nanohedra" strategy[22,23] using symmetry to design the nanostructures. The design of a dimer−trimer PN-Block is notably a versatile and powerful approach as a geometrically based building block to construct several polyhedra with three edges from one node, such as a


DOI: 10.1021/jacs.5b03593
J. Am. Chem. Soc. 2015, 137, 11285−11293

tetrahedron, hexahedron, and dodecahedron. The WA20-foldon fusion protein was constructed as a fundamental PN-Block by fusing the dimeric *de novo* protein WA20 and trimeric foldon domain of T4 phage fibritin[6,43] with an alanine-rich short linker (the amino-acid sequence: KLAAA) (Figure 1 and Figure S2, Supporting Information). The residues in this linker have relatively high helix-forming propensities.[55] The foldon domain consisting of only 26 residues is suitable for a trimeric connecting vertex/node part because it promotes stable trimerization by fast folding,[6] and its application to the construction of engineered bionanotubes was reported.[56] In the stable self-assembling complexes of the WA20-foldon, it is expected to form several oligomers in multiples of 6-mer because of the combination of the WA20 dimer and foldon trimer (Figure 1C).

**Self-Assembling Oligomers of WA20-Foldon Produced in *E. coli*.** The WA20-foldon protein with a $His_6$ tag was expressed in a soluble fraction in *E. coli* and purified by IMAC. Sodium dodecyl sulfate polyacrylamide gel electrophoresis (SDS-PAGE) of the purified fraction shows almost a single band (Figure 2A). However, native PAGE of the same fraction shows several discrete bands (Figure 2B), suggesting that the WA20-foldon forms several homooligomeric states simultaneously in the soluble fraction in *E. coli*. The stable WA20-foldon oligomers were further purified by SEC, and the four discrete bands were separated in native PAGE (Figure 2D), but they showed the same single band in SDS-PAGE (Figure 2C). The major discrete bands of the WA20-foldon oligomers were named the small form (S form), middle form (M form), large form (L form), and huge form (H form) in order from the lower band in native PAGE (Figure 2D). In addition, Figure S6 (Supporting Information) shows that the quality of the proteins did not change practically in SDS-PAGE and native PAGE after at least ~8 months of storage at 4 °C, suggesting that the WA20-foldon protein is very stable at the level of not only the polypeptide but also its oligomeric states (i.e., no observable exchange between the forms).

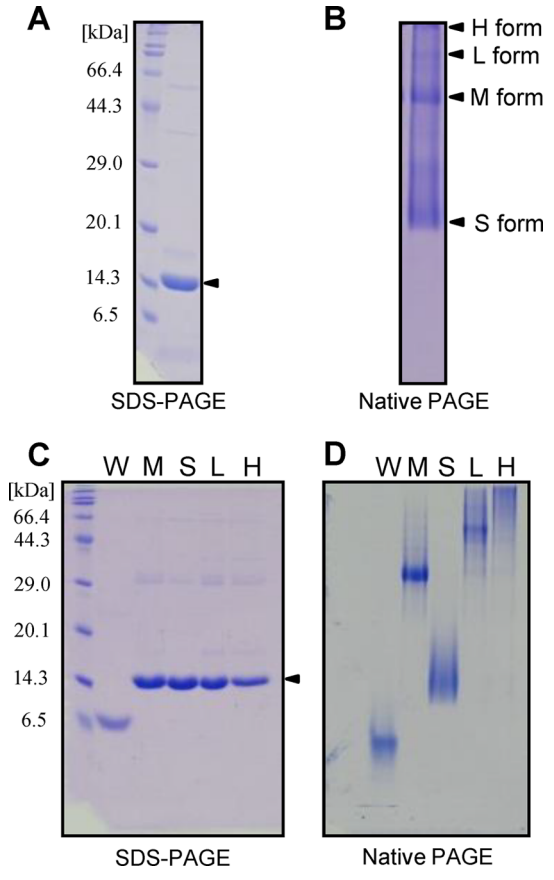


**Figure 2.** Polyacrylamide gel electrophoresis of WA20-foldon. (A) SDS-PAGE (17.5% polyacrylamide gel) and (B) native PAGE (7.5% polyacrylamide gel) of the WA20-foldon after IMAC purification. (C) SDS-PAGE (17.5% gel) and (D) native PAGE (7.5% gel) of each form of the WA20-foldon after SEC purification. S: S form; M: M form; L: L form; H: H form; W: WA20 as a control sample. Proteins were stained with Coomassie brilliant blue. The protein molecular weight marker (broad) (Takara Bio, Otsu, Japan) was used for SDS-PAGE.

**Analyses of Oligomeric States of WA20-Foldon.** To estimate the molecular mass of the WA20-foldon oligomers, we first analyzed each form of the purified WA20-foldon using SEC. Figure 3 shows the chromatograms of each form of the WA20-foldon. The peaks of the S and M forms are sharp and nearly symmetrical-shaped single peaks, suggesting that they are almost monodispersed. In contrast, the peak shapes of the L and H forms are broad, suggesting that they are polydispersed. Table 1 shows the elution volume and estimated molecular mass using SEC with the standard calibration curve (Figure S7, Supporting Information). The molecular masses of the individual forms of the WA20-foldon were estimated to be 84 kDa (S form), 195 kDa (M form), 284 kDa (L form), and 415

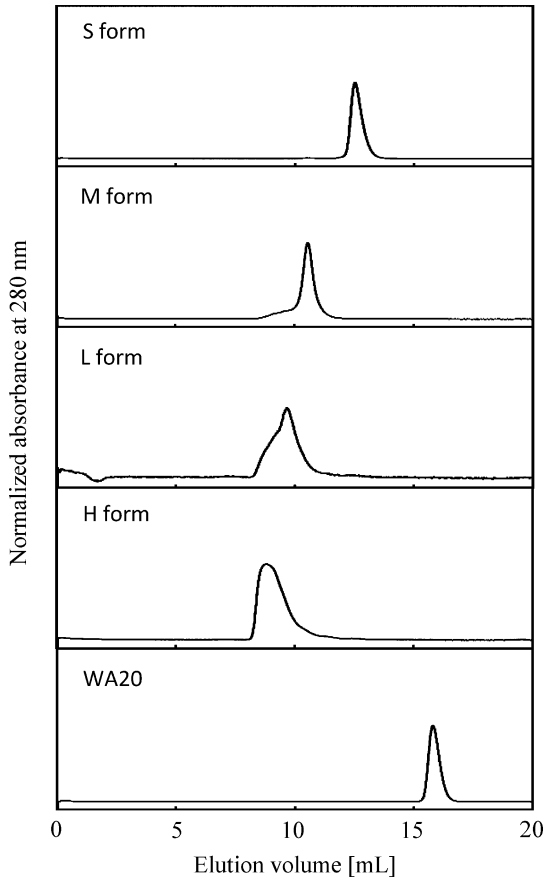


**Figure 3.** SEC chromatograms of each form of the purified WA20-foldon on Superdex 200 Increase 10/300 GL. WA20 was used as a control sample. The elution volume and molecular mass, estimated by the standard calibration curve (Figure S7, Supporting Information) are summarized in Table 1.


DOI: 10.1021/jacs.5b03593
J. Am. Chem. Soc. 2015, 137, 11285−11293

**Table 1. Elution Volume and Estimated Molecular Mass of WA20-Foldon Oligomers in SEC Experiments**

| sample | elution volume [mL] | $M_w$ [kDa] | oligomeric state [mer][a] |
|---|---|---|---|
| S form | 12.5 | 84.0 | 5 |
| M form | 10.6 | 195 | 11 |
| L form | 9.7 | 284 | 17 |
| H form | 8.8 | 415 | 24 |
| WA20 | 15.8 | 21.0 | 2 |

[a]The molecular mass of a WA20-foldon protomer is 17.0 kDa.

kDa (H form). However, the molecular mass of the H form might be underestimated because the H form peak overlapped with the column void volume (8.5 mL, elution volume of Blue Dextran 2000). Because the molecular mass of a WA20-foldon protomer is 17.0 kDa, oligomeric states of the individual forms of the WA20-foldon were roughly calculated to be 5-mer (S form), 11-mer (M form), 17-mer (L form), and 24-mer (H form) (Table 1).

To determine the absolute molecular mass without reference standard samples, we performed SEC-MALS[57] experiments (Table 2; and Figure S8, Supporting Information). The molecular masses of the individual forms of the WA20-foldon were determined to be 101 kDa (S form), 199 kDa (M form), 299 kDa (L form), 392 kDa ($H_1$ form: the lower-mass refined component in the H form), and 543 kDa ($H_2$ form: the higher-mass refined component in the H form), and their oligomeric states were estimated to be 6-mer (S form), 12-mer (M form), 18-mer (L form), 23-mer ($H_1$ form), and 32-mer ($H_2$ form). These results suggest that the WA20-foldon forms regularly discrete oligomers in multiples of 6-mer because of the combination of the WA20 dimer and foldon trimer (Figure 1C).

**Table 2. Molecular Mass of WA20-Foldon Oligomers Determined by SEC-MALS Experiments**

| sample | $M_w$ [kDa] | oligomeric state [mer] |
|---|---|---|
| S form | 101 | 6 |
| M form | 199 | 12 |
| L form | 299 | 18 |
| $H_1$ form | 392 | 23 |
| $H_2$ form | 543 | 32 |

As the third independent method to analyze molecular mass of the WA20-foldon oligomers, we performed AUC experiments. First, we performed sedimentation velocity experiments (Figure S9, Supporting Information). The $c(s)$ distribution of the sample S shows the presence of a single species corresponding to the S form with a sedimentation coefficient ($s_{20,w}$) of 5.20 (±0.02) S (Figure S9A, Supporting Information). The molecular mass was estimated to be 91 (±2) kDa. The frictional ratio, $f/f_0$, for the S form was calculated to be 1.45 (±0.02). The value of the frictional ratio represents the degree of deviation, due to hydration, rugosity, asymmetry, and expansion of the molecule. The S form has a larger frictional ratio of 1.45 than the typical values of 1.05−1.30 for globular proteins,[58] implying that it has an atypical shape (e.g., an elongated shape).

The $c(s)$ distribution of the sample M shows the presence of two main species corresponding to the M and S forms (Figure S9B, Supporting Information). The large peak has a sedimentation coefficient ($s_{20,w}$) of 7.61 (±0.01) S for the M form, and another small peak has that of 5.34 (±0.02) S for the S form. Because the $c(s)$ distribution shape, the sedimentation coefficient value, and the ratio of the peak height did not significantly change with the protein concentration, the two species are independent molecules, not in equilibrium system (i.e., self-association system and/or subunit exchanging system), in the time scale of the experiments.

The $c(s)$ distribution of the sample L shows that the solution contains various species in the broad range (Figure S9C, Supporting Information). The major peak has a sedimentation coefficient ($s_{20,w}$) of 9.93 (±0.04) S probably for the L form and another peak has that of 6.49 (±0.02) S. However, these values may possess lower reliability because the peaks are small and broad. Also, the $c(s)$ distribution of the sample H shows that the solution contains various species (Figure S9D, Supporting Information). It is difficult to analyze this because of the small and broad peaks.

Judging from the results of sedimentation velocity experiments, we further performed sedimentation equilibrium AUC experiments of the samples S and M to determine molecular mass of the S and M forms of the WA20-foldon (Figure 4). The molecular mass of the S form was determined to be 96 (±1) kDa from the sedimentation equilibrium experiments of the sample S (Figure 4A). The molecular masses of the two species in the sample M were determined to be 180 (±8) kDa for the M form and 100 (±5) kDa for the S form from the sedimentation equilibrium experiments using two species analysis model (Figure 4B). From these results, the oligomeric states of the S and M forms were estimated to be 6-mer and 11-mer, respectively.

In addition, the matrix-assisted laser desorption/ionization time-of-flight (MALDI-TOF) mass spectrum of the S form of the WA20-foldon cross-linked by glutaraldehyde shows the mass peak of $m/z$ = 111449 assignable to 6-mer considering mass increase due to chemical modification (Figure S10, Supporting Information). However, mass spectra peaks of the other forms of the WA20-foldon were not observed probably because of the higher molecular masses of the M, L, and H forms.

Furthermore, Figure 5A shows SAXS intensities of a series of the WA20-foldon oligomers, WA20, and chicken egg lysozyme. Assuming that these proteins have practically identical scattering length densities and specific volumes and that the structure factor $S(q) \approx 1$ for dilute samples, the forward-scattering intensity normalized by protein concentration, $I(q \rightarrow 0)/c$, is proportional to the weight-average molecular mass ($M_w$). Lysozyme ($M_w$ = 14.3 kDa) was used as a molecular mass reference standard. The average molecular masses of the individual forms of the WA20-foldon were estimated to be 97.1 kDa (S form), 224 kDa (M form), 331 kDa (L form), and 641 kDa (H form), and oligomeric states of the individual forms of the WA20-foldon were roughly calculated to be 6-mer (S form), 13-mer (M form), 19-mer (L form), and 38-mer (H form) (Table 3).

Table 4 summarizes the results of molecular mass and oligomeric states of the WA20-foldon oligomers, determined by the multifaceted experiments. Because the stable form of the WA20-foldon should form the oligomers in multiples of 6-mer in the light of the combination of the WA20 dimer and foldon trimer, overall these results indicate that the individual forms of the WA20-foldon exist as hexamer (6-mer) for the S form, dodecamer (12-mer) for the M form, octadecamer (18-mer)


DOI: 10.1021/jacs.5b03593
J. Am. Chem. Soc. 2015, 137, 11285−11293

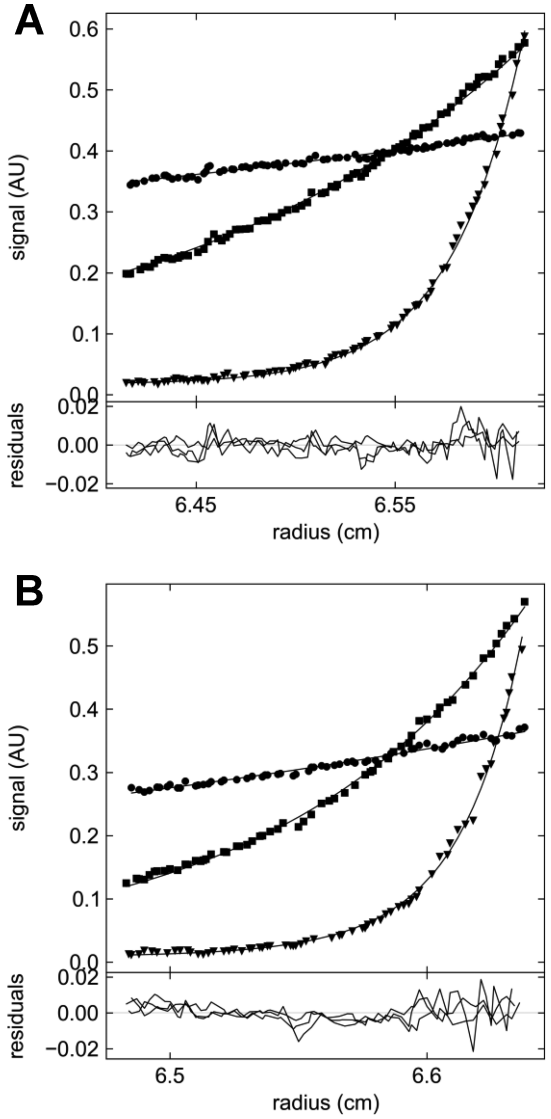


**Figure 4.** Sedimentation equilibrium AUC experiments of the WA20-foldon. Scans from three different rotor speeds (●: 4000 rpm; ■: 9000 rpm; ▼: 20000 rpm) monitored at 280 nm. (Protein concentration: 0.3 mg/mL). (A) Sample S: the lines represent fits to the data of a single species model that yield a calculated protein mass of 96 kDa. (B) Sample M: the lines represent fits to the data of two species model that yield calculated protein mass of 100 and 180 kDa.

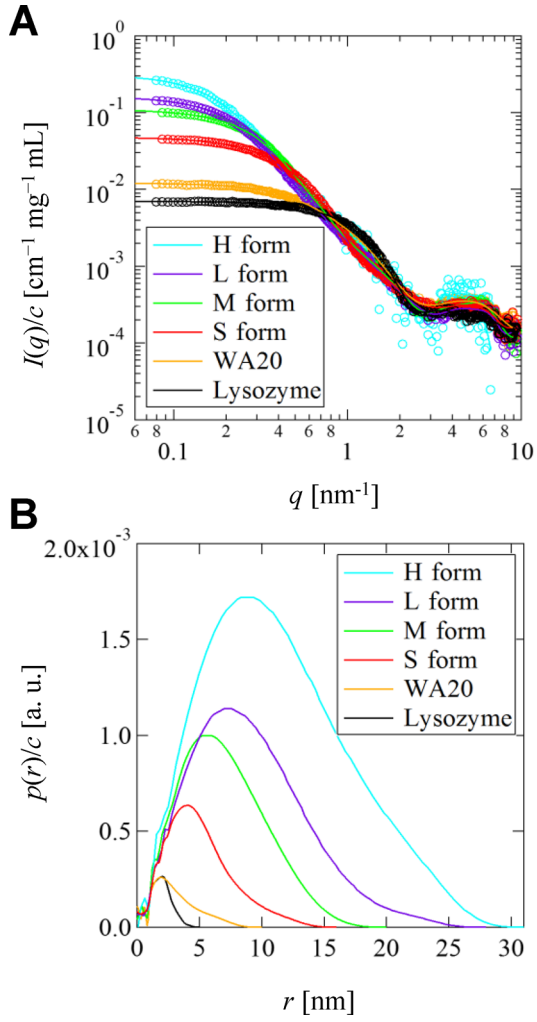


**Figure 5.** SAXS analysis of the WA20-foldon. (A) Concentration-normalized absolute scattering intensities, $I(q)/c$, of the WA20-foldon oligomers, lysozyme, and WA20. (B) Their real-space information, pair-distance distribution functions normalized by the concentration, $p(r)/c$, as obtained by IFT.

for the L form, and a mixture of 24-mer, 30-mer, and perhaps higher oligomers for the H form.

**Shape Analysis of WA20-Foldon from SAXS Data.** To extract intuitive real-space information from the SAXS data, the pair-distance distribution functions, $p(r)$, reflected by the shapes of the WA20-foldon oligomers were obtained using the IFT technique[49−51] (Figure 5B). The integral of $p(r)/c$ from $r = 0$ to $r = D_{max}$ is equal to the extrapolated forward absolute scattering intensity normalized by concentration, $I(q \rightarrow 0)/c$, and therefore, it is proportional to the weight-average molecular mass, $M_w$. The shape of $p(r)$ of the S form is characterized by an extended tail in the high-$r$ regime, which is approximated by an ellipsoid.[50] In contrast, $p(r)$ of the M form shows a comparatively symmetrical bell-like shape, suggesting a sphere-like structure. The shapes of $p(r)$ of the L and H forms show a higher similarity to that of the M form than that of the S form. These suggest that the L and H forms exist in larger sphere-like structures. However, the high-$r$ residual of $p(r)$ of the L form implies that the L form contains a larger-sized complex as a minor component because of its polydispersity, as suggested by the SEC experiment (Figure 3).

**Table 3. SAXS Analysis Data and Estimated Molecular Mass of WA20-Foldon Oligomers**

| sample | $I(q\rightarrow0)/c$ [$cm^{-1}$ $mg^{-1}$ mL] | $D_{max}$ [nm] | $R_g$ [nm] | $M_w$ [kDa] | oligomeric state [mer] |
|---|---|---|---|---|---|
| S form | 0.048 | 16 | 3.9 | 97.1 | 6 |
| M form | 0.11 | 20 | 5.3 | 224 | 13 |
| L form | 0.16 | 28 | 6.9 | 331 | 19 |
| H form | 0.31 | 31 | 8.7 | 641 | 38 |
| WA20 | 0.012 | 10 | 2.5 | 24.6 | 2 |
| lysozyme[a] | 0.0070 | 5.0 | 1.5 | 14.3 | 1 |

[a]Lysozyme is as a molecular mass reference standard.

Because of further purification by repeated SEC, the S and M forms of the WA20-foldon can be considered as practically monodispersed particles. Therefore, further analysis for the S and M forms was performed to obtain more structural insights from the SAXS data utilizing high-resolution structures of the


DOI: 10.1021/jacs.5b03593
J. Am. Chem. Soc. 2015, 137, 11285−11293

**Table 4. Summary of Molecular Mass and Oligomeric State of WA20-Foldon Oligomers**

| form | SEC | MALS | AUC | MS | SAXS | oligomeric state [mer][a] |
|---|---|---|---|---|---|---|
| S form | 84 | 101 | 96 | 111 | 97 | 6 |
| M form | 195 | 199 | 180 | – | 224 | 12 |
| L form | 284 | 299 | – | – | 331 | 18 |
| H form | 415 | 392, 543 | – | – | 641 | 24, 30, 36? |

[a]The molecular mass of a WA20-foldon protomer is 17.0 kDa.

WA20 and foldon domains with geometrical and symmetrical restrictions. The rigid-body model structures of the S form hexamer and the M form dodecamer were iteratively constructed based on the crystal structure of the dimeric WA20 (PDB code 3VJF)[5] and the NMR structure of the trimeric foldon domain (PDB code 1RFO)[6] to reproduce the experimental $p(r)$ and $I(q)$ (Figures S3–S5, Supporting Information). The models were constructed with a consideration of linking their C and N terminals with two- and three-fold symmetries (Figures S3 and S4, Supporting Information). The models show the extended barrel-like structure for the S form (Figure 6A) and the distinctive tetrahedron-like structure for the M form (Figure 7A). The $p(r)$ and $I(q)$ simulated from the models of the S and M forms closely resemble those obtained from the SAXS experiments (Figures 6B and 7B and Figure S5, Supporting Information). Moreover, the hydrodynamic properties of the S and M forms are predicted from the rigid-body model structures using the program HYDRO-PRO.[59] The predicted radii of gyration ($R_g$) are 3.9 nm (S form) and 5.0 nm (M form), and the predicted sedimentation coefficients ($s_{20,w}$) are 5.4 S (S form) and 7.9 S (M form). These values are highly consistent with the experimental results, 3.9 nm (S form) and 5.3 nm (M form) of $R_g$ from SAXS and 5.2 S (S form) and 7.6 S (M form) of $s_{20,w}$ from AUC, supporting our rigid-body models.

Furthermore, the low-resolution shapes of the S and M forms were reconstructed from the SAXS data using the *ab initio* modeling program DAMMIN.[53] The protein models were composed of small beads (dummy atoms). The shapes were estimated using nonlinear least-squares that fit the experimental SAXS data (Figures 6D and 7D). We performed calculations several times with and without symmetry constraints (*P*2 and/or *P*3, derived from the dimer and/or trimer domains, respectively), and a majority of the calculations led to similar results. The typical and major results are shown in Figures 6C and 7C. The S form shows an elongated barrel-like shape (Figure 6C). The M form shows a less-elongated, sphere-like shape with four humps, similar to a tetrahedron, with a consideration of a *P*23 symmetry constraint (Figure 7C).

**Perspectives of PN-Block Approach.** We demonstrated that the WA20-foldon fusion protein as a PN-Block formed several types of self-assembling oligomeric nanostructures. The results illustrated the concept of the "PN-Block approach": various self-assembling nanostructures are created from a few types of simple and fundamental PN-Blocks (Figure 1). PN-Blocks using the intermolecularly folded dimeric *de novo* protein (e.g., WA20) have some advantages: (1) the simple, stable, and intertwined rod-like structure of the *de novo* protein makes it easy to use PN-Blocks to design and construct simple and stable frameworks of nanoarchitectures, and (2) the PN-Blocks using the *de novo* protein, based on the simple binary patterning, have great potential for redesigning functional nanostructures using our functional binary-patterned *de novo* protein library.[16,60] ("PN" in PN-Block also has a different meaning from the polar and nonpolar abbreviations used in the binary code strategy for protein design.) Moreover, the PN-

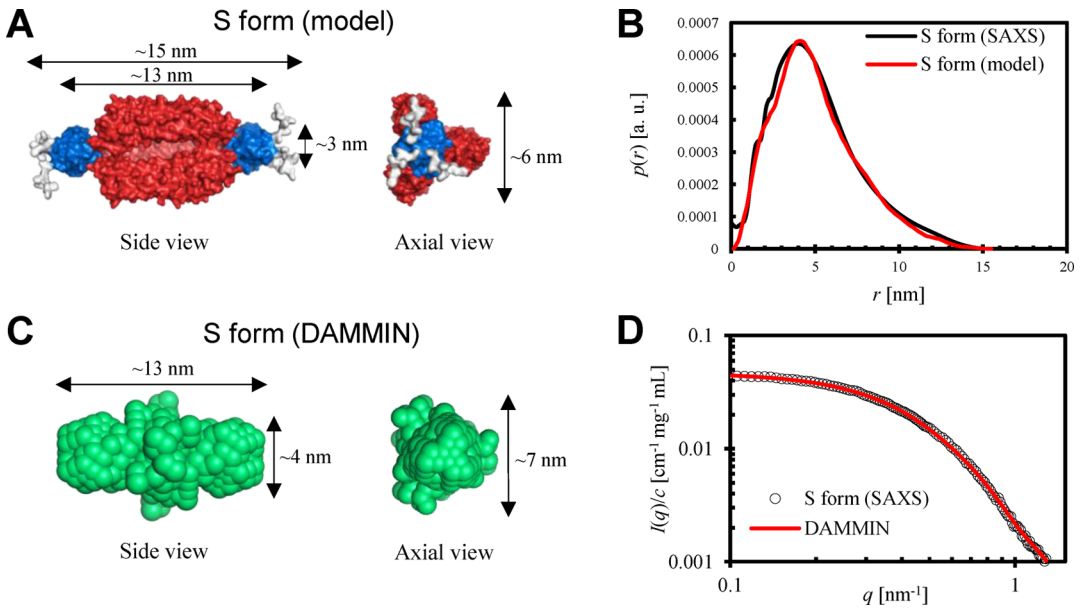


**Figure 6.** Three-dimensional model structures of the S form of the WA20-foldon derived from SAXS analysis. (A) The rigid-body model structure of the S form hexamer of the WA20-foldon. The domains of the WA20 (PDB code 3VJF),[5] foldon (PDB code 1RFO),[6] and $His_6$ tag are shown in red, blue, and light gray, respectively. (B) The pair-distance distribution function, $p(r)$, of the S form of the WA20-foldon as obtained by the SAXS experiment (black line) and that simulated from the rigid-body model structure (red line). (C) The dummy atom model shape of the S form of the WA20-foldon reconstructed from the SAXS data using the *ab initio* modeling program DAMMIN with a *P*32 symmetry constraint.[53] (D) The concentration-normalized SAXS intensity, $I(q)/c$, of the S form of the WA20-foldon (black open circle) and that optimized by the DAMMIN procedure (red line).



DOI: 10.1021/jacs.5b03593
J. Am. Chem. Soc. 2015, 137, 11285–11293

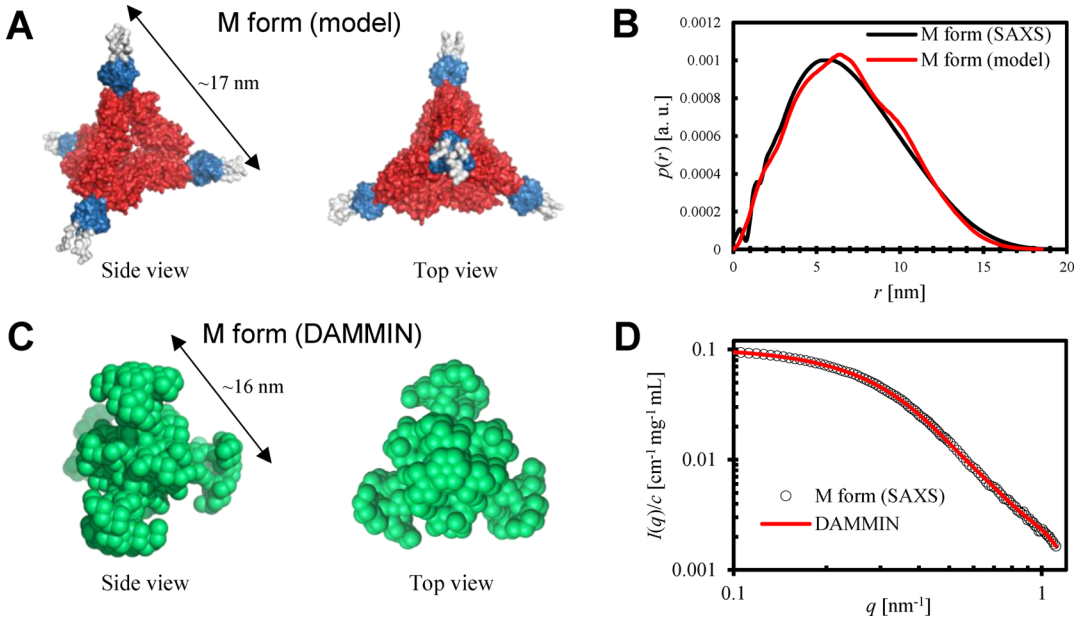


**Figure 7.** Three-dimensional model structures of the M form of the WA20-foldon derived from SAXS analysis. (A) The rigid-body model structure of the M form dodecamer of the WA20-foldon. The domains are shown in the same colors as in Figure 6A. (B) The pair-distance distribution function, $p(r)$, of the M form of the WA20-foldon as obtained by the SAXS experiment (black line) and that simulated from the rigid-body model structure (red line). (C) The dummy atom model shape of the M form of the WA20-foldon reconstructed from the SAXS data using the program DAMMIN with a *P*23 symmetry constraint. (D) The concentration-normalized SAXS intensity, $I(q)/c$, of the M form of the WA20-foldon (black open circle) and that optimized by the DAMMIN procedure (red line).

Block approach can be further enhanced by adding cofactors and/or synthetic ligands such as metal-directed protein self-assemblies[31,32] and the protein encapsulation in synthetic self-assembled coordination cages[61] and by using computational methods for protein design such as Rosetta software suite for macromolecular modeling.[62,63]

## CONCLUSIONS

In this study, we designed and developed the self-assembling WA20-foldon fusion protein as a novel protein nanobuilding block (PN-Block) using the intermolecularly folded dimeric *de novo* protein WA20. The study revealed that the WA20-foldon, as one PN-Block, simultaneously formed several distinctive types of self-assembling homooligomers in multiples of 6-mer because of the combination of the WA20 dimer and foldon trimer. The SAXS analyses suggest that the S and M forms of the WA20-foldon exist in nanostructures of a barrel-like-shaped hexamer and tetrahedron-like-shaped dodecamer, respectively. These results demonstrate that the PN-Block approach using the intertwined dimeric *de novo* protein is a powerful strategy to create self-assembling supramolecular nanoarchitectures.

## ASSOCIATED CONTENT

### Supporting Information

Additional results, Tables S1 and S2, Figures S1–S10, and related descriptions. The Supporting Information is available free of charge on the ACS Publications website at DOI: 10.1021/jacs.5b03593.

## AUTHOR INFORMATION

### Corresponding Author

*rarai@shinshu-u.ac.jp

### Notes

The authors declare no competing financial interest.

## ACKNOWLEDGMENTS

We thank Dr. Nobuyasu Koga and Dr. Rie Koga at the Institute for Molecular Science (IMS) for assistance in SEC-MALS experiments. We also thank Prof. Nobuaki Hayashida at Shinshu University for helpful advice. This work was supported by the Joint Studies Program (2014–2015) of IMS. Preliminary experiments related to this work were performed at Photon Factory (PF), KEK, under the approval of PF program advisory committee (proposal no. 2014G111). We are indebted to Divisions of Gene Research and Instrumental Analysis of Research Center for Human and Environmental Sciences, Shinshu University, for providing facilities. This work was supported by JSPS Research Fellowships (DC2) and Grant-in-Aid for JSPS Fellows to N.K. and Grant-in-Aid for Scientific Research (KAKENHI grant nos. 22113508, 24113707, and 24780097), JSPS Postdoctoral Fellowships for Research Abroad, and Program for Dissemination of Tenure-Track System, to R.A., funded by JSPS and MEXT, Japan. The work was also supported by NSF Grants MCB-1050510 and MCB-1409402 to M.H.H.

## REFERENCES

(1) Seeman, N. C. *Nature* **2003**, *421*, 427.
(2) Rothemund, P. W. *Nature* **2006**, *440*, 297.
(3) Endo, M.; Yang, Y.; Sugiyama, H. *Biomater. Sci.* **2013**, *1*, 347.
(4) Ke, Y. *Curr. Opin. Struct. Biol.* **2014**, *27*, 122.
(5) Arai, R.; Kobayashi, N.; Kimura, A.; Sato, T.; Matsuo, K.; Wang, A. F.; Platt, J. M.; Bradley, L. H.; Hecht, M. H. *J. Phys. Chem. B* **2012**, *116*, 6789.
(6) Guthe, S.; Kapinos, L.; Moglich, A.; Meier, S.; Grzesiek, S.; Kiefhaber, T. *J. Mol. Biol.* **2004**, *337*, 905.
(7) Dahiyat, B. I.; Mayo, S. L. *Science* **1997**, *278*, 82.
(8) Kuhlman, B.; Dantas, G.; Ireton, G. C.; Varani, G.; Stoddard, B. L.; Baker, D. *Science* **2003**, *302*, 1364.



DOI: 10.1021/jacs.5b03593
*J. Am. Chem. Soc.* 2015, 137, 11285–11293

(9) Koga, N.; Tatsumi-Koga, R.; Liu, G.; Xiao, R.; Acton, T. B.; Montelione, G. T.; Baker, D. *Nature* **2012**, *491*, 222.
(10) Keefe, A. D.; Szostak, J. W. *Nature* **2001**, *410*, 715.
(11) Kamtekar, S.; Schiffer, J. M.; Xiong, H.; Babik, J. M.; Hecht, M. H. *Science* **1993**, *262*, 1680.
(12) Hecht, M. H.; Das, A.; Go, A.; Bradley, L. H.; Wei, Y. *Protein Sci.* **2004**, *13*, 1711.
(13) West, M. W.; Wang, W.; Patterson, J.; Mancias, J. D.; Beasley, J. R.; Hecht, M. H. *Proc. Natl. Acad. Sci. U. S. A.* **1999**, *96*, 11211.
(14) Wei, Y.; Liu, T.; Sazinsky, S. L.; Moffet, D. A.; Pelczer, I.; Hecht, M. H. *Protein Sci.* **2003**, *12*, 92.
(15) Bradley, L. H.; Kleiner, R. E.; Wang, A. F.; Hecht, M. H.; Wood, D. W. *Protein Eng., Des. Sel.* **2005**, *18*, 201.
(16) Patel, S. C.; Bradley, L. H.; Jinadasa, S. P.; Hecht, M. H. *Protein Sci.* **2009**, *18*, 1388.
(17) Bennett, M. J.; Choe, S.; Eisenberg, D. *Proc. Natl. Acad. Sci. U. S. A.* **1994**, *91*, 3127.
(18) Bennett, M. J.; Schlunegger, M. P.; Eisenberg, D. *Protein Sci.* **1995**, *4*, 2455.
(19) Glykos, N. M.; Cesareni, G.; Kokkinidis, M. *Structure* **1999**, *7*, 597.
(20) Peters, K.; Hinz, H. J.; Cesareni, G. *Biol. Chem.* **1997**, *378*, 1141.
(21) Ogihara, N. L.; Ghirlanda, G.; Bryson, J. W.; Gingery, M.; DeGrado, W. F.; Eisenberg, D. *Proc. Natl. Acad. Sci. U. S. A.* **2001**, *98*, 1404.
(22) Padilla, J. E.; Colovos, C.; Yeates, T. O. *Proc. Natl. Acad. Sci. U. S. A.* **2001**, *98*, 2217.
(23) Lai, Y. T.; Cascio, D.; Yeates, T. O. *Science* **2012**, *336*, 1129.
(24) Lai, Y. T.; Tsai, K. L.; Sawaya, M. R.; Asturias, F. J.; Yeates, T. O. *J. Am. Chem. Soc.* **2013**, *135*, 7738.
(25) Sinclair, J. C.; Davies, K. M.; Venien-Bryan, C.; Noble, M. E. *Nat. Nanotechnol.* **2011**, *6*, 558.
(26) Pandya, M. J.; Spooner, G. M.; Sunde, M.; Thorpe, J. R.; Rodger, A.; Woolfson, D. N. *Biochemistry* **2000**, *39*, 8728.
(27) Papapostolou, D.; Smith, A. M.; Atkins, E. D.; Oliver, S. J.; Ryadnov, M. G.; Serpell, L. C.; Woolfson, D. N. *Proc. Natl. Acad. Sci. U. S. A.* **2007**, *104*, 10853.
(28) Sharp, T. H.; Bruning, M.; Mantell, J.; Sessions, R. B.; Thomson, A. R.; Zaccai, N. R.; Brady, R. L.; Verkade, P.; Woolfson, D. N. *Proc. Natl. Acad. Sci. U. S. A.* **2012**, *109*, 13266.
(29) Boyle, A. L.; Bromley, E. H.; Bartlett, G. J.; Sessions, R. B.; Sharp, T. H.; Williams, C. L.; Curmi, P. M.; Forde, N. R.; Linke, H.; Woolfson, D. N. *J. Am. Chem. Soc.* **2012**, *134*, 15457.
(30) Fletcher, J. M.; Harniman, R. L.; Barnes, F. R.; Boyle, A. L.; Collins, A.; Mantell, J.; Sharp, T. H.; Antognozzi, M.; Booth, P. J.; Linden, N.; Miles, M. J.; Sessions, R. B.; Verkade, P.; Woolfson, D. N. *Science* **2013**, *340*, 595.
(31) Salgado, E. N.; Faraone-Mennella, J.; Tezcan, F. A. *J. Am. Chem. Soc.* **2007**, *129*, 13374.
(32) Brodin, J. D.; Ambroggio, X. I.; Tang, C.; Parent, K. N.; Baker, T. S.; Tezcan, F. A. *Nat. Chem.* **2012**, *4*, 375.
(33) Gradisar, H.; Bozic, S.; Doles, T.; Vengust, D.; Hafner-Bratkovic, I.; Mertelj, A.; Webb, B.; Sali, A.; Klavzar, S.; Jerala, R. *Nat. Chem. Biol.* **2013**, *9*, 362.
(34) King, N. P.; Sheffler, W.; Sawaya, M. R.; Vollmar, B. S.; Sumida, J. P.; Andre, I.; Gonen, T.; Yeates, T. O.; Baker, D. *Science* **2012**, *336*, 1171.
(35) King, N. P.; Bale, J. B.; Sheffler, W.; McNamara, D. E.; Gonen, S.; Gonen, T.; Yeates, T. O.; Baker, D. *Nature* **2014**, *510*, 103.
(36) Armstrong, C. T.; Boyle, A. L.; Bromley, E. H. C.; Mahmoud, Z. N.; Smith, L.; Thomson, A. R.; Woolfson, D. N. *Faraday Discuss.* **2009**, *143*, 305.
(37) Salgado, E. N.; Radford, R. J.; Tezcan, F. A. *Acc. Chem. Res.* **2010**, *43*, 661.
(38) Radford, R. J.; Brodin, J. D.; Salgado, E. N.; Tezcan, F. A. *Coord. Chem. Rev.* **2011**, *255*, 790.
(39) Woolfson, D. N.; Bartlett, G. J.; Bruning, M.; Thomson, A. R. *Curr. Opin. Struct. Biol.* **2012**, *22*, 432.
(40) Lai, Y. T.; King, N. P.; Yeates, T. O. *Trends Cell Biol.* **2012**, *22*, 653.
(41) King, N. P.; Lai, Y. T. *Curr. Opin. Struct. Biol.* **2013**, *23*, 632.
(42) Bozic, S.; Doles, T.; Gradisar, H.; Jerala, R. *Curr. Opin. Chem. Biol.* **2013**, *17*, 940.
(43) Tao, Y.; Strelkov, S. V.; Mesyanzhinov, V. V.; Rossmann, M. G. *Structure* **1997**, *5*, 789.
(44) Pace, C. N.; Vajdos, F.; Fee, L.; Grimsley, G.; Gray, T. *Protein Sci.* **1995**, *4*, 2411.
(45) Laue, T. M.; Shah, B. D.; Ridgeway, T. M.; Pelletier, S. L. In *Analytical Ultracentrifugation in Biochemistry and Polymer Science*; Harding, S. E., Rowe, A. J., Horton, J. C., Eds.; Royal Society of Chemistry: Cambridge, UK, 1992; p 90.
(46) Schuck, P. *Biophys. J.* **2000**, *78*, 1606.
(47) Vistica, J.; Dam, J.; Balbo, A.; Yikilmaz, E.; Mariuzza, R. A.; Rouault, T. A.; Schuck, P. *Anal. Biochem.* **2004**, *326*, 234.
(48) Orthaber, D.; Bergmann, A.; Glatter, O. *J. Appl. Crystallogr.* **2000**, *33*, 218.
(49) Glatter, O. *J. Appl. Crystallogr.* **1980**, *13*, 577.
(50) Glatter, O.; Kratky, O. *Small-Angle X-Ray Scattering*; Academic Press: New York, 1982.
(51) Brunner-Popela, J.; Glatter, O. *J. Appl. Crystallogr.* **1997**, *30*, 431.
(52) Emsley, P.; Lohkamp, B.; Scott, W. G.; Cowtan, K. *Acta Crystallogr., Sect. D: Biol. Crystallogr.* **2010**, *66*, 486.
(53) Svergun, D. I. *Biophys. J.* **1999**, *76*, 2879.
(54) Petoukhov, M. V.; Franke, D.; Shkumatov, A. V.; Tria, G.; Kikhney, A. G.; Gajda, M.; Gorba, C.; Mertens, H. D. T.; Konarev, P. V.; Svergun, D. I. *J. Appl. Crystallogr.* **2012**, *45*, 342.
(55) Pace, C. N.; Scholtz, J. M. *Biophys. J.* **1998**, *75*, 422.
(56) Yokoi, N.; Inaba, H.; Terauchi, M.; Stieg, A. Z.; Sanghamitra, N. J.; Koshiyama, T.; Yutani, K.; Kanamaru, S.; Arisaka, F.; Hikage, T.; Suzuki, A.; Yamane, T.; Gimzewski, J. K.; Watanabe, Y.; Kitagawa, S.; Ueno, T. *Small* **2010**, *6*, 1873.
(57) Wyatt, P. J. *Anal. Chim. Acta* **1993**, *272*, 1.
(58) Tanford, C. *Physical Chemistry of Macromolecules*; Wiley: New York, 1961.
(59) Ortega, A.; Amoros, D.; Garcia de la Torre, J. *Biophys. J.* **2011**, *101*, 892.
(60) Fisher, M. A.; McKinley, K. L.; Bradley, L. H.; Viola, S. R.; Hecht, M. H. *PLoS One* **2011**, *6*, e15364.
(61) Fujita, D.; Suzuki, K.; Sato, S.; Yagi-Utsumi, M.; Yamaguchi, Y.; Mizuno, N.; Kumasaka, T.; Takata, M.; Noda, M.; Uchiyama, S.; Kato, K.; Fujita, M. *Nat. Commun.* **2012**, *3*, 1093.
(62) Leaver-Fay, A.; Tyka, M.; Lewis, S. M.; Lange, O. F.; Thompson, J.; Jacak, R.; Kaufman, K.; Renfrew, P. D.; Smith, C. A.; Sheffler, W.; Davis, I. W.; Cooper, S.; Treuille, A.; Mandell, D. J.; Richter, F.; Ban, Y. E.; Fleishman, S. J.; Corn, J. E.; Kim, D. E.; Lyskov, S.; Berrondo, M.; Mentzer, S.; Popovic, Z.; Havranek, J. J.; Karanicolas, J.; Das, R.; Meiler, J.; Kortemme, T.; Gray, J. J.; Kuhlman, B.; Baker, D.; Bradley, P. *Methods Enzymol.* **2011**, *487*, 545.
(63) Baker, D. *Biochem. Soc. Trans.* **2014**, *42*, 225.


DOI: 10.1021/jacs.5b03593
*J. Am. Chem. Soc.* 2015, 137, 11285−11293